Green Synthesis of Hybrid Papain/$Ni_3(PO_4)_2$ Rods Electrocatalyst for Enhanced Oxygen Evolution Reaction

Imtiaz Ahmed[a], Rathindranath Biswas[a], Harjinder Singh[a], Ranjit A. Patil[b], Rohit Varshney[c], Debabrata Patra[c], Yuan-Ron Ma[b] and Krishna Kanta Haldar[a]*

[a]Department of Chemistry, Central University of Punjab, Bathinda, 151401, India.
[b]Department of Physics, National Dong Hwa University, Hualien 97401, Taiwan.
[c]Institute of Nano Science and Technology, Mohali, 160062, India.

*Author to whom correspondence should be addressed; electronic Email: krishankant.haldar@cup.edu.in.

Instrumentations:

ATR-FTIR were performed using Bruker (Model: Vertex 70v) ATR spectrometer. Raman spectra were acquired with a confocal Raman microscope (Witec alpha 300 R) using a 532 nm laser equipped with an upright optical microscope (Zeiss). Powder X-ray diffraction (PXRD) pattern was obtained on a Bruker D8 Advances instrument using Cu-Kα (λ = 1.5406 Å) radiation in the 2θ range from 10° to 80° with an acceleration voltage of 40KV (Detector used = Xcelerator FASS ID detector and voltage = 45 kV). FESEM instrument was used to perceive scanning electron microscopy (SEM) images (Carl Zeiss, Voltage = 20 kV). X-ray photoelectron spectroscopy (XPS) measurements were performed using the Thermo Scientific Inc. System equipped with a microfocus monochromatic Al Kα X-ray source of energy ~1450 e. All electrochemical measurements were performed with Metrohm Autolab (M204 multichannel potentiostat galvanostat using Nova 2.1.4 software. Brunauer-Emmett-Teller (BET) measurement was carried out with Make-Quanta Chrome instruments, Model: AutosorbiQ and ASiQwin. High Resolution Transmission Electron Microscope (HR-TEM) images was taken by Technai G2s Twin, Model FEI, and Raman spectra were acquired with a confocal Raman microscope (Witec alpha 300 R) using a 532 nm laser equipped with an upright optical microscope (Zeiss).

Preparation of electrodes:

The excellent properties of Papain/$Ni_3(PO_4)_2$ catalyst for OER in alkaline, neutral and acidic electrolyte make it promising catalyst for electrocatalytic water splitting. Catalyst ink was prepared by wisely crushing the mixture of Papain/$Ni_3(PO_4)_2$ using a mortar and pestle in which 4 mg of the finely ground product was taken in a 0.5 mL solution containing a mixture of ethanol (200 μL) and deionized water (300 μL) and sonicated for 30 minutes. Then, 25 μL of the binder was carefully added and sonicate again for 10 minutes thereafter 5 μL drop-coated over a GC (glassy carbon) electrode, and it was dried under mild vacuum condition for overnight.

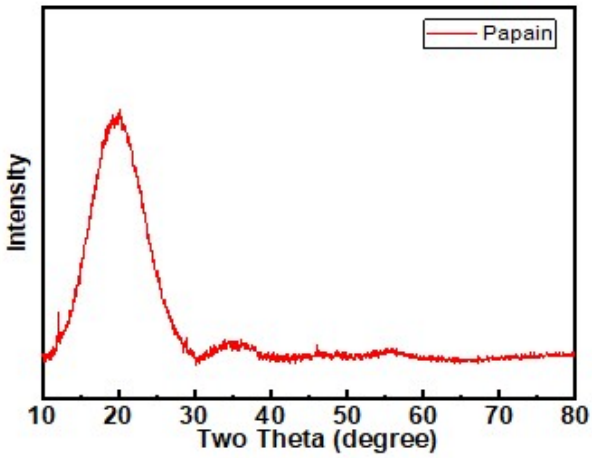

Figure S1. Powder XRD pattern of Papain.

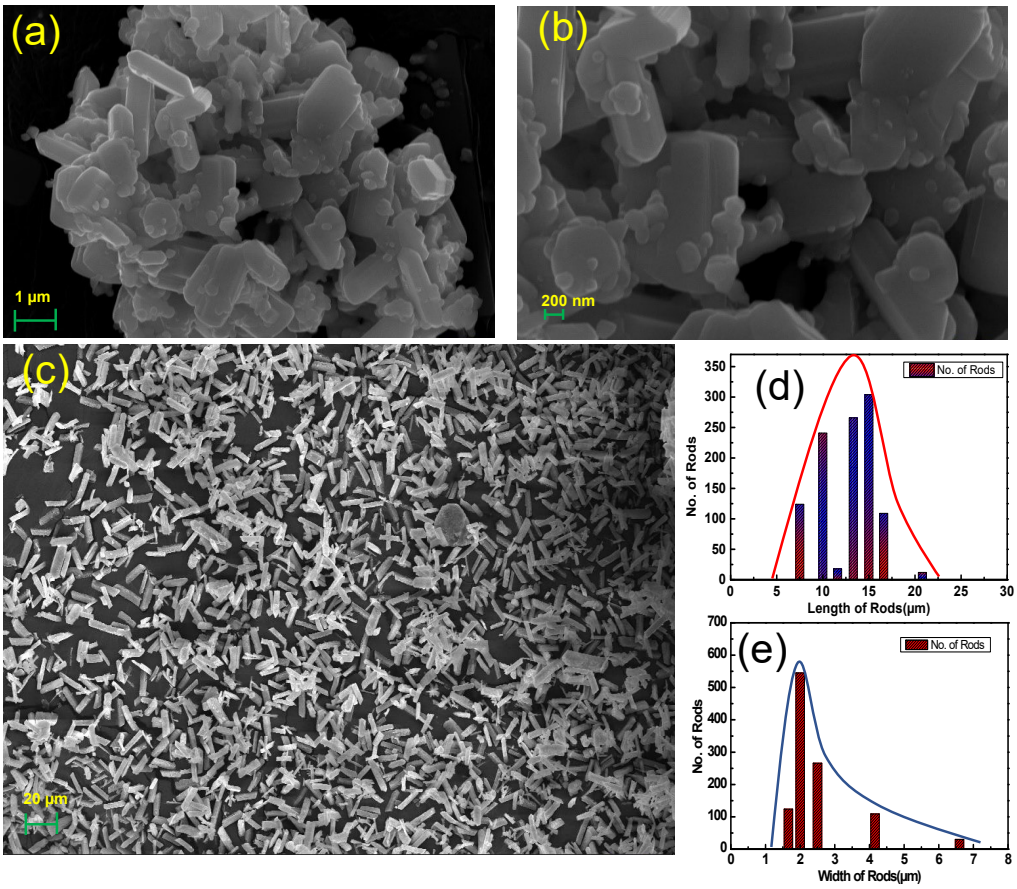

Figure S2. (a) and (b) different magnification FE-SEM images of $Ni_3(PO_4)_2$ nanostructures synthesised in absence of Papain extract. (c) FE-SEM image and (d, e) are particle size (length and width) distribution histogram of Papain/$Ni_3(PO_4)_2$.

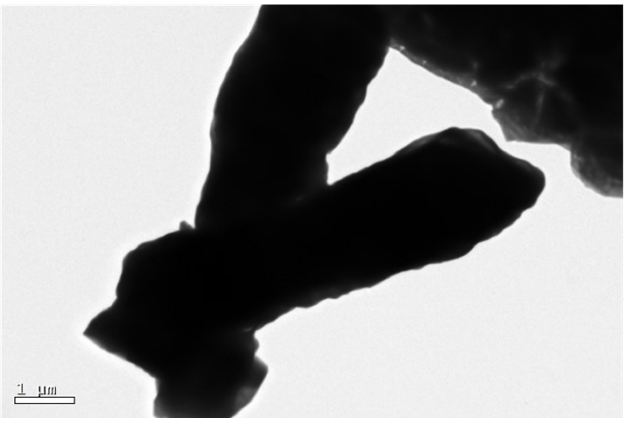

Figure S3. TEM image of Papain/$Ni_3(PO_4)_2$@700 ºC microrods using 1 mL of Papain extract.

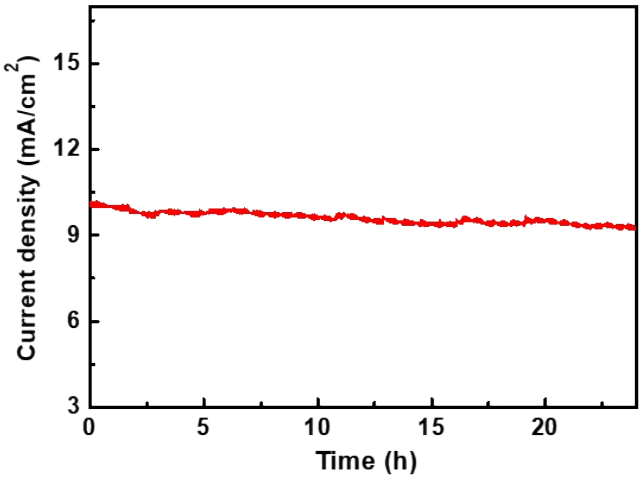

Figure S4. Chronoamperometry method of Papain/$Ni_3(PO_4)_2$ composite at an overpotential of 217 mV for 24 hours.

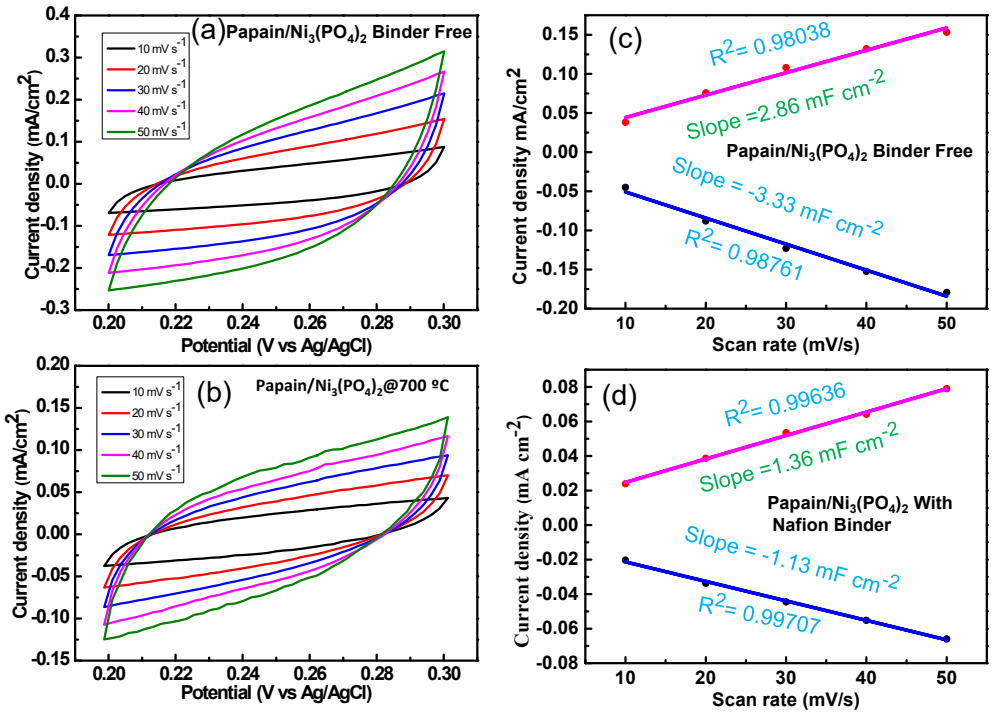

Figure S5. Cyclic voltammetry curves of (a) Papain/$Ni_3(PO_4)_2$ and (b) and $Ni_3(PO_4)_2$ (c-d) are their corresponding plot of J_a and J_c against scan rate for the determination of double layer capacitance (C_{dl}) of the catalysts, respectively.

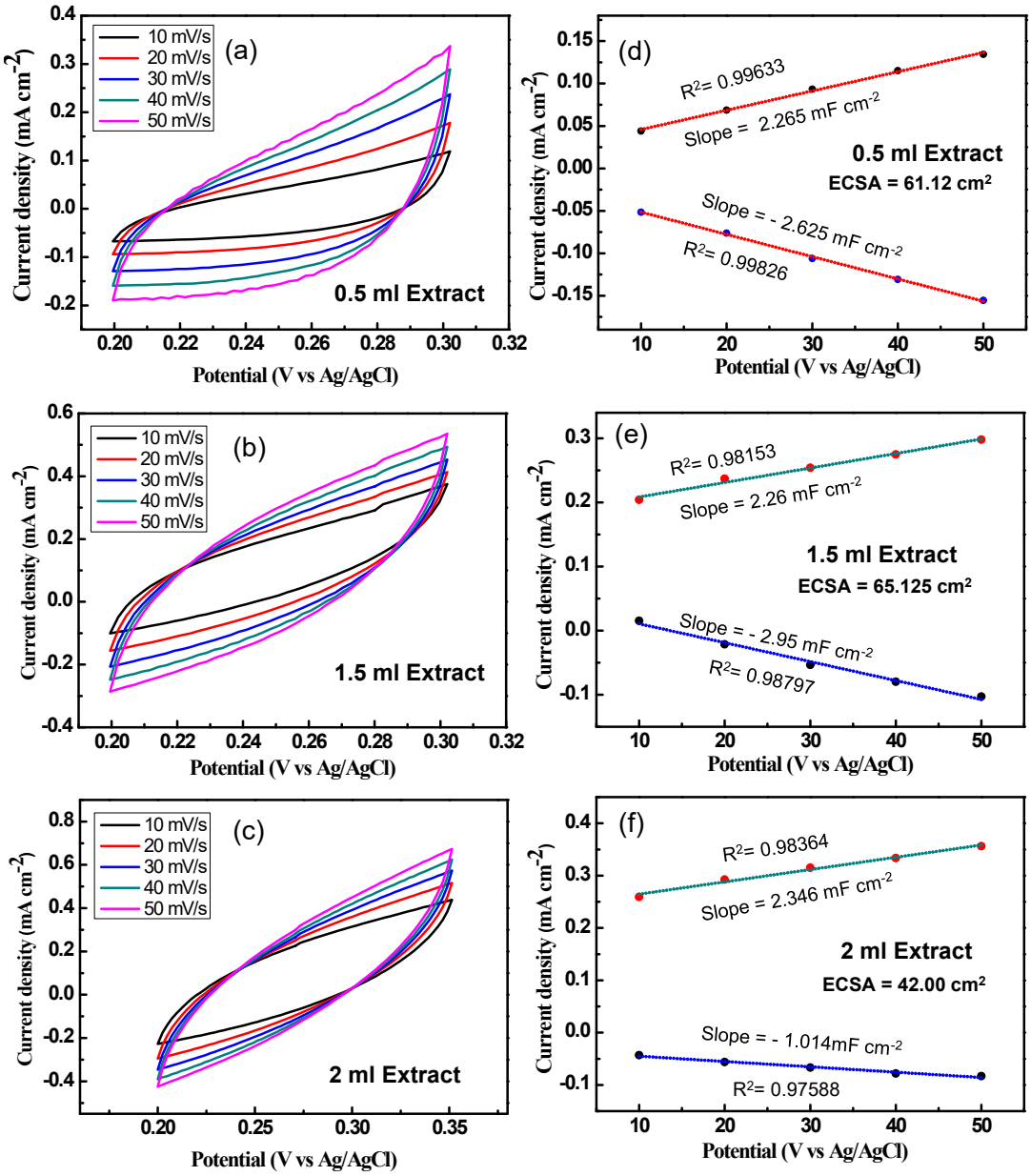

Figure S6. (a-c) Cyclic voltammetry curves and (d-f) are their corresponding plot of J_a and J_c against scan rate for the determination of double layer capacitance (C_{dl}) of as synthesised Papain/$Ni_3(PO_4)_2$ using 0.5, 1, and 2 ml of Papain extract, respectively.

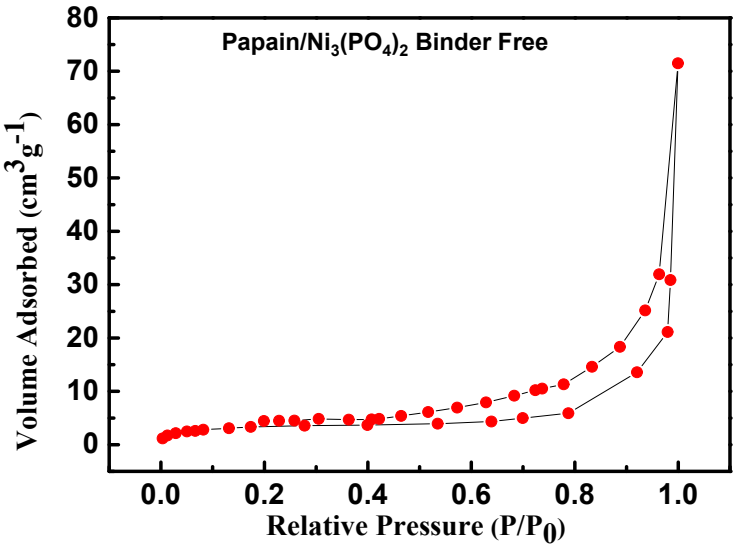

Figure S7: The N_2 adsorption-desorption isotherm of Papain/$Ni_3(PO_4)_2$ composite microstructures catalyst.

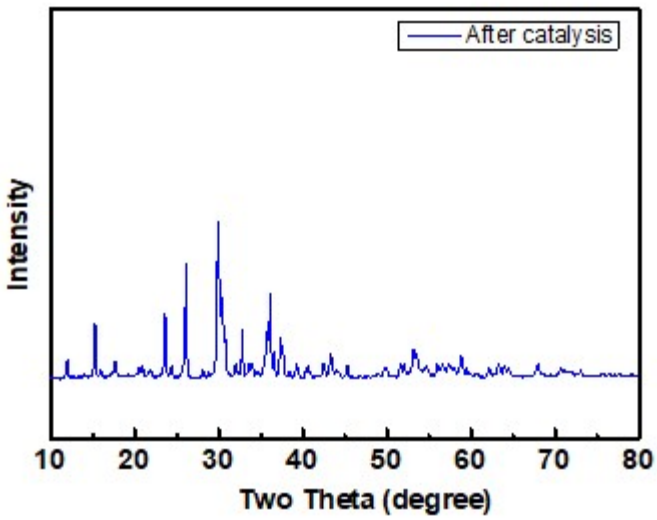

Figure S8. (a) Post catalytic powder XRD pattern of Papain/$Ni_3(PO_4)_2$ microstructures.

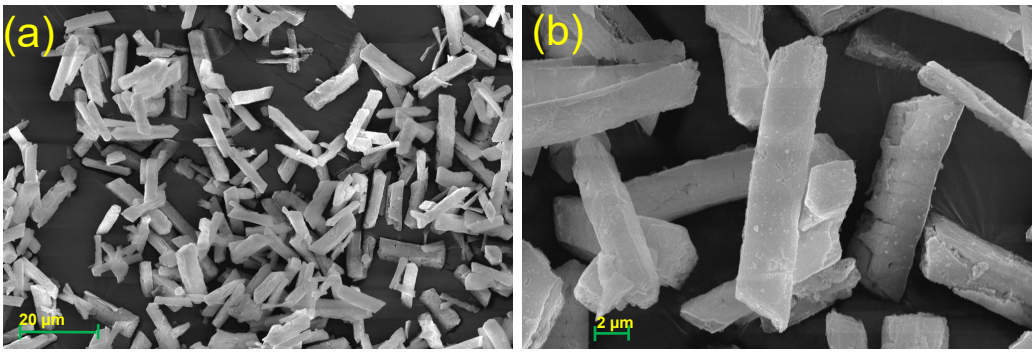

Figure S9. (a), and (b) High magnification FE-SEM images of Papain/$Ni_3(PO_4)_2$ composite microstructures after chronoamperometry stability test for OER activity.

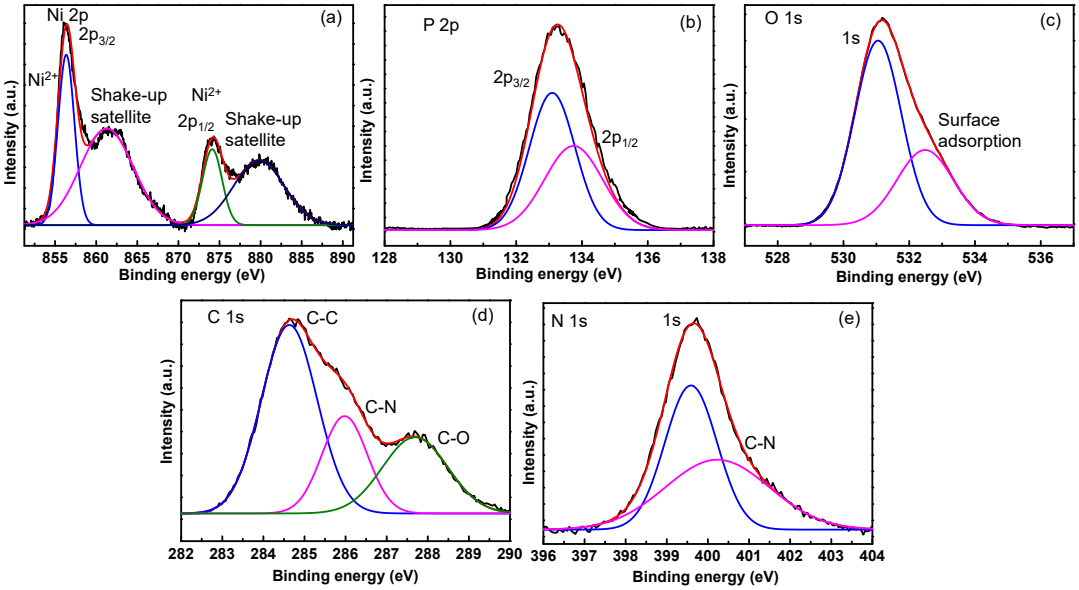

Figure S10. After catalysis high-resolution deconvoluted XPS spectra of (a) Ni 2p, (b) P 2p, (c) O 1s (d) C 1s, and (e) N 1s core-levels in Papain/$Ni_3(PO_4)_2$ composite structure.

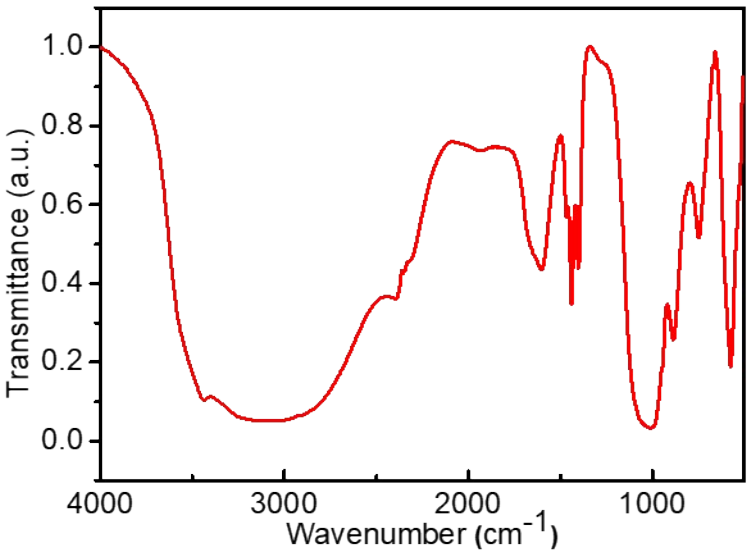

Figure S11. Post catalytic FT-IR of Papain/$Ni_3(PO_4)_2$ microstructures.

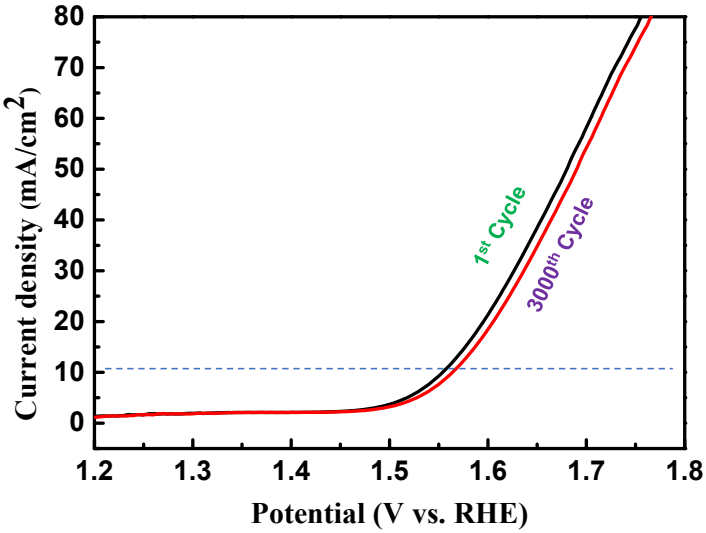

Figure S12. Polarization curves of composite of 1st and 3000th cycles of continuous operation in neutral condition.

Table S1. Comparison of OER activity of Papain/$Ni_3(PO_4)_2$ hybrid nanostructure with some reported Nickel- based catalysts in an alkaline medium.

Catalyst	Overpotential (mV) at 10 mA/cm^2	Tafel slope (mV dec^{-1})	Electrolyte used	Reference
NiO/Ni-foam	300 mV	98 mV/dec	1 M KOH	1
CoMoNiSNF-31	166 mV	58 mV/dec	1 M KOH	2
$NiCo_2O_4$/NiCoP	295 mV	70 mV/dec	1 M KOH	3
NiCoP	338 mV	78 mV/dec	1 M KOH	3
$NiCo_2O_4$	384 mV	80 mV/dec	1 M KOH	3
Co_9S_8/Ni_3S_2/NF	192 mV	70 mV/dec	1 M KOH	2
MoS_2/Ni_3S_2/NF	239 mV	71 mV/dec	1 M KOH	2
Ni_3S_2/NF	395 mV	74 mV/dec	1 M KOH	2
$Ni_{12}P_5/Ni_3(PO_4)_2$-SS	378 mV	78.6 mV/dec	1 M KOH	4
$Ni_{12}P_5/Ni_3(PO_4)_2$-HS	318 mV	69.8 mV/dec	1 M KOH	4
NiO/CN	281 mV	66.37 mV/dec	1 M KOH	5
NiO@MoO_3/VC	280 mV	64.5 mV/dec	1 M KOH	6
NiCoP/CC	242 mV	64.2 mV/dec	1 M KOH	7
Ni-NiO/N-rGO	240 mV	43 mV/dec	0.1 M KOH	8
NCNT/CoO-NiO-NiCo	270 mV	40 mV/dec	1 M KOH	9
NiS/NF	320 mV	71 mV/dec	1 M KOH	10
Papain/$Ni_3(PO4)_2$	217 mV	63 mV/dec		**This work**

Determination of Turn Over Frequency (TOF)

The TOF value for OER performance can be calculated as described equation (4) [52-54]

$$TOF = \frac{j\,N_A}{F\,n\,\Gamma} \qquad \text{---------- (4)}$$

Where,

j = current density (mA cm^{-2}), N_A = Avogadro constant ($6.0221 \times 10^{23}\ mole^{-1}$), n is the number of electrons transferred = 4, and Γ is the surface or total concentration of catalyst in terms of number of atoms.

Surface area of GC = 0.07065 cm^2

Mass loading catalyst on GC = 0.193 mg/cm^2 = (0.193 mg/cm^2 × 0.07065 cm^2) = 0.01364 mg = 1.36×10^{-5} g

Surface concentration of Ni (Γ): (6.7128×10^{16} atoms/surface area of GC) = 9.5015×10^{17} atoms cm^{-2}.

TOF value for OER experiment at overpotential of 310 mV (1.54 V vs. RHE):

$$TOF_{1.54\,V} = \frac{j\,N_A}{F\,n\,\Gamma} = \frac{39.03 \times 10^{-3}\ A\,cm^{-2}\ \times (6.0221 \times 10^{23}\ atoms\ mole^{-1})}{96485\ s\,A\,mole^{-1}\ \times 4\ \times (9.5015 \times 10^{17}\ atoms\ cm^{-2})}$$

$$TOF_{1.54\,V} = 0.06409\ s^{-1}$$

Number of Ir atoms present on GC surface = 6.0655×10^{-8} mole = $6.0655\times10^{-8} \times 6.0221\times10^{23}$ = 3.6527×10^{16}

Surface concentration (Γ): (3.6527×10^{16}/surface area of GC) = 5.1701×10^{17} atoms cm^{-2}.

TOF IrO_2 for OER at an overpotential of 310 mV:

$$TOF_{1.54\,V} = \frac{j\,N_A}{F\,n\,\Gamma} = \frac{3.8\times10^{-3}\,A\,cm^{-2}\ \times(6.0221\times10^{23}\,atoms\,mole^{-1})}{96485\,s\,A\,mole^{-1}\ \times 4\ \times(5.1701\times10^{17}\,atoms\,cm^{-2})}$$

$$= 0.01146\ s^{-1}$$

References

1. Khalid, S.; Cao, C.; Ahmad, A.; Wang, L.; Tanveer, M.; Aslam, I.; Tahir, M.; Idrees, F.; Zhu, Y., Microwave assisted synthesis of mesoporous $NiCo_2O_4$ nanosheets as electrode material for advanced flexible supercapacitors. *Rsc Advances* **2015,** *5* (42), 33146-33154.
2. Yang, Y.; Yao, H.; Yu, Z.; Islam, S. M.; He, H.; Yuan, M.; Yue, Y.; Xu, K.; Hao, W.; Sun, G., Hierarchical nanoassembly of $MoS_2/Co_9S_8/Ni_3S_2/Ni$ as a highly efficient electrocatalyst for overall water splitting in a wide pH range. *Journal of the American Chemical Society* **2019,** *141* (26), 10417-10430.
3. Jin, W.; Chen, J.; Wu, H.; Zang, N.; Li, Q.; Cai, W.; Wu, Z., Interface engineering of oxygen-vacancy-rich $NiCo_2O_4$/NiCoP heterostructure as an efficient bifunctional electrocatalyst for overall water splitting. *Catalysis Science & Technology* **2020,** *10* (16), 5559-5565.
4. Chang, J.; Lv, Q.; Li, G.; Ge, J.; Liu, C.; Xing, W., Core-shell structured $Ni1_2P_5/Ni_3\,(PO_4)_2$ hollow spheres as difunctional and efficient electrocatalysts for overall water electrolysis. *Applied Catalysis B: Environmental* **2017,** *204*, 486-496.
5. Liao, C.; Yang, B.; Zhang, N.; Liu, M.; Chen, G.; Jiang, X.; Chen, G.; Yang, J.; Liu, X.; Chan, T. S., Constructing conductive interfaces between nickel oxide nanocrystals and polymer carbon nitride for efficient electrocatalytic oxygen evolution reaction. *Advanced Functional Materials* **2019,** *29* (40), 1904020.
6. Illathvalappil, R.; George, L.; Kurungot, S., Coexisting few-layer assemblies of NiO and MoO_3 deposited on vulcan carbon as an efficient and durable electrocatalyst for water oxidation. *ACS Applied Energy Materials* **2019,** *2* (7), 4987-4998.
7. Du, C.; Yang, L.; Yang, F.; Cheng, G.; Luo, W., Nest-like NiCoP for highly efficient overall water splitting. *Acs Catalysis* **2017,** *7* (6), 4131-4137.
8. Liu, X.; Liu, W.; Ko, M.; Park, M.; Kim, M. G.; Oh, P.; Chae, S.; Park, S.; Casimir, A.; Wu, G., Metal (Ni, Co)-metal oxides/graphene nanocomposites as multifunctional electrocatalysts. *Advanced Functional Materials* **2015,** *25* (36), 5799-5808.
9. Liu, X.; Park, M.; Kim, M. G.; Gupta, S.; Wu, G.; Cho, J., Integrating NiCo alloys with their oxides as efficient bifunctional cathode catalysts for rechargeable zinc–air batteries. *Angewandte Chemie International Edition* **2015,** *54* (33), 9654-9658.
10. Ren, J.-T.; Yuan, Z.-Y., Hierarchical nickel sulfide nanosheets directly grown on Ni foam: a stable and efficient electrocatalyst for water reduction and oxidation in alkaline medium. *ACS Sustainable Chemistry & Engineering* **2017,** *5* (8), 7203-7210.